

Impact of Interatomic Electronic Decay Processes on Xe 4d Hole Decay in the Xenon Fluorides

Christian Buth,* Robin Santra,† and Lorenz S. Cederbaum

Theoretische Chemie, Physikalisch-Chemisches Institut, Ruprecht-Karls-Universität Heidelberg,
Im Neuenheimer Feld 229, 69120 Heidelberg, Germany

(Dated: 19 March 2003)

A hole in a 4d orbital of atomic xenon relaxes through Auger decay after a lifetime of 3 fs. Adding electronegative fluorine ligands to form xenon fluoride molecules, results in withdrawal of valence-electron density from Xe. Thus, within the one-center picture of Auger decay, a lowered Xe 4d Auger width would be expected, in contradiction, however, with experiment. Employing extensive *ab initio* calculations within the framework of many-body Green's functions, we determine all available decay channels in XeF_n and characterize these channels by means of a two-hole population analysis. We derive a relation between two-hole population numbers and partial Auger widths. On this basis, interatomic electronic decay processes are demonstrated to be so strong in the xenon fluorides that they overcompensate the reduction in intra-atomic Auger width and lead to the experimentally observed trend. The nature of the relevant processes is discussed. These processes presumably underlie Auger decay in a variety of systems.

I. INTRODUCTION

The Auger effect^{1,2,3,4,5} provides a magnificent means to study atoms, molecules, and surfaces. It is caused by a special type of electronic resonance, i.e., the decay by electron emission of core-ionized atoms, molecules, or solids. Since its discovery it has received much attention, because it is a fundamental process yielding deep insights into complex many-body effects in matter. Moreover, the Auger effect has proven to be useful in many experimental situations^{2,3,4,5,6} and can be used as an analytical tool. Therefore, an in-depth understanding of the Auger effect is important both for fundamental and practical reasons.

A particularly interesting situation arises when systems consisting of more than one atom are considered. Can the Auger decay rate of a core hole in an atom be influenced—or maybe even adjusted at will—by modifying the chemical environment of that atom? If yes, what are the underlying mechanisms? Early experiments on gas-phase molecules⁷ and ionic solids⁸ hinted at a simple correlation between the binding energy of a core electron and the Auger width of the associated core hole. For instance, withdrawal of valence electrons by electronegative ligands induces a chemical shift of the core level toward higher binding energies; at the same time, a smaller number of valence electrons is available for Auger decay, if a local, atomic mechanism is assumed. Hence, within the one-center picture of Auger decay⁹, an increase in binding energy is accompanied by a decrease in Auger width.

Citrin¹⁰, however, analyzed x-ray photoemission measurements in a number of metal oxides and halides, and found convincing evidence for interatomic processes, which can lead to a trend in contradiction to the one-center model. Citrin's work stimulated theoretical work on interatomic Auger decay in crystalline NaCl¹¹ and NaF.¹² Matthew and Komninos¹³ were the first to present a formal examination of interatomic Auger processes. Using strong approximations,⁶ they concluded

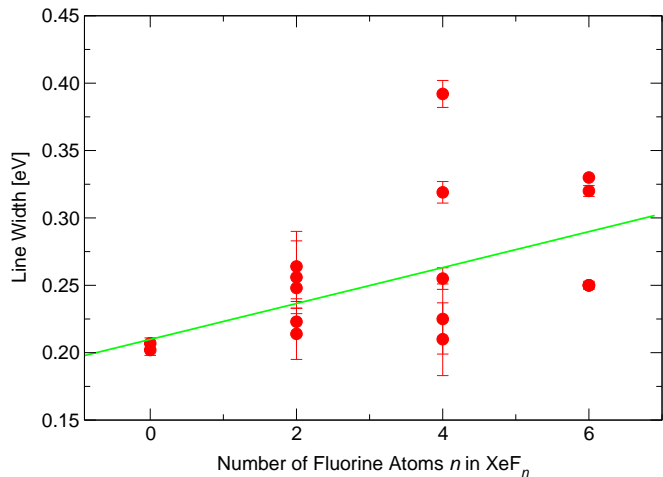


FIG. 1: Experimental widths of the Xe 4d lines in Xe, XeF_2 , XeF_4 , and XeF_6 ¹⁹. The figure²⁰ suggests an average increase of the linewidth with an increasing number of fluorine atoms. Note that due to spin-orbit coupling and ligand-field effects, the Xe 4d orbitals are not all equivalent.

that these transitions have a small impact on the Auger rate, except in low-energy Auger processes. In fact, recent theoretical and experimental investigations show that in the low-energy case the effect of the chemical bond can be dramatic.^{14,15,16,17,18}

In this work, we argue that interatomic electronic decay processes can have an even greater impact than previously assumed. We investigate as an example Auger decay of a Xe 4d hole in Xe, XeF_2 , XeF_4 , and XeF_6 . It is demonstrated that the Auger width in the series XeF_n , $n = 0, 2, 4, 6$, would decrease drastically if only intra-atomic decay played a role. By contrast, the experimentally observed linewidths¹⁹ display—in clear contradiction to the one-center picture mentioned previously—a monotonic increase from Xe to XeF_6 . This is illustrated

in Fig. 1.²⁰ We show that interatomic Auger processes are responsible for the discrepancy. Vibrational broadening, which could cause a similar effect, is very likely to be insignificant.¹⁹ Single ionization spectra of the xenon fluorides, which we have calculated recently,^{21,22} provided a first theoretical indication of an entirely electronic mechanism.

The xenon fluorides constitute, from our point of view, an ideal example, because of the relatively weak bonding between the central noble-gas atom and the fluorine ligands. This allows us to identify various interatomic decay processes and to distinguish them from the intra-atomic one. In particular, the purely interatomic/intermolecular electronic decay mechanisms that govern the inner-valence physics in weakly bound clusters of atoms or molecules^{23,24,25,26,27,28,29} provide a conceptual framework for our analysis. Therefore, a short summary of these processes is given in Sec. II.

The nature of Auger decay in a molecule can be assessed most clearly by characterizing the available decay channels. To this end, Sec. III introduces a many-body Green's function method—the algebraic diagrammatic construction scheme^{16,30}—for calculating double ionization spectra of molecules at a highly correlated level. A two-hole population analysis^{14,31} is discussed that serves as an important tool for determining the localization properties of the two holes in an Auger decay channel. Using Wigner-Weisskopf theory,^{32,33} we derive a relationship between final-state population numbers and partial Auger widths. The calculated double ionization spectra are analyzed in Sec. IV, and the relevance of interatomic decay processes for the decay of $\text{Xe}4d$ vacancies is elucidated. Concluding remarks are the subject of Sec. V.

II. ELECTRONIC DECAY PROCESSES IN WEAKLY BOUND SYSTEMS

In this section, we review the knowledge obtained in the study of the electronic decay of inner-valence ionized clusters. The decay processes discovered in clusters, and the associated terminology we use in order to emphasize the nature of the underlying mechanisms, allow a succinct classification of the Auger processes in XeF_n . We mention that the decay processes discussed in the following for singly ionized systems can be generalized to describe the decay of inner-valence vacancies of multiply ionized clusters.^{25,34}

Intra-atomic electronic decay (IAED) is usually the most prominent electronic decay process of core-ionized atoms embedded in molecules or clusters. IAED is, of course, the only Auger process that can take place in an isolated atom. In atoms, this mechanism is well understood.^{1,2,3,4,5} The initial core hole is filled by a (valence) electron and the excess energy is transferred via Coulomb interaction to a second (valence) electron, which is emitted subsequently [Fig. 2(a)]. In molecules or clusters,

intra-atomic decay is not the only decay process, because other processes can occur that involve neighboring atoms or molecules.

If one removes an inner-valence electron from an isolated atom or molecule, the ionized system cannot, in general, decay by electron emission, for it lies energetically below the double ionization threshold. The situation changes if the monomer is part of a cluster.

The initial inner-valence vacancy is filled by a valence electron of the same monomer and the excess energy is transferred to a second valence electron of a neighboring monomer. This electron is emitted subsequently. See Fig. 2(b) for a schematic representation. The decay process is termed *interatomic* or *intermolecular Coulombic decay* (ICD) for clusters of atoms or clusters of molecules, respectively. It was identified theoretically in several weakly bound clusters: $(\text{HF})_n$ clusters,^{23,25,27,35} the $\text{HF}(\text{H}_2\text{O})_2$ cluster,³⁶ $(\text{H}_2\text{O})_n$ clusters,²³ Ne_n clusters,^{24,28,37} and the NeAr dimer.²⁶ Further we would like to point out studies of electronic decay after inner-valence ionization of CN^{-38} and of fluorinated carbanions and their acids.³⁹

ICD of inner-valence holes in clusters is ultrafast, typically taking place on a time scale of the order of 10 fs (see Ref. 40 for a review). Experimental evidence for ICD has been found recently in neon clusters.²⁹ In the context of this paper, it is especially important to note that ICD is highly sensitive to cluster size: The ICD width in Ne_n clusters, for instance, increases strongly with n , when a central neon atom carries the initial inner-valence vacancy and the surrounding atoms converge with n to the shape of the first coordination sphere in solid neon.²⁸ Clearly, a larger number of nearest neighbors translates into a larger number of dicationic decay channels available for ICD.

The ionization spectra of neon and argon are quantitatively very different from one another (Ref. 26, and references therein). Neon has significantly higher lying single (IP) and double ionization potentials (DIP) compared to argon. The inner-valence $\text{Ne}2s$ IP is larger than the $\text{Ne}^{-1}\text{Ar}^{-1}$ DIP in the NeAr dimer.²⁶ Therefore, an initial $\text{Ne}2s$ vacancy can lead to ICD. However, the $\text{Ne}2s$ vacancy in NeAr can decay in another way, too, because the $\text{Ne}2s$ IP is also larger than the NeAr^{-2} DIP. In this case, a valence electron from argon drops into the $\text{Ne}2s$ hole and the excess energy is transferred to another valence electron of argon. Upon electron emission, the dimer is left in a NeAr^{-2} state. This process is called *electron-transfer mediated decay* (ETMD).²⁶ A schematic representation of the ETMD process is shown in Fig. 2(c). In Ref. 26 it is shown that the contribution of ETMD to the total electronic decay width of an initial $\text{Ne}2s$ vacancy in NeAr is appreciably smaller than the contribution of ICD. In light of the vastly increasing ICD width in neon clusters,²⁸ we expect a similar size effect for ETMD, too. In the ETMD described, only two atoms are involved. It is called *two-monomer ETMD* (ETMD2).

A *three-monomer ETMD* (ETMD3) has been sug-

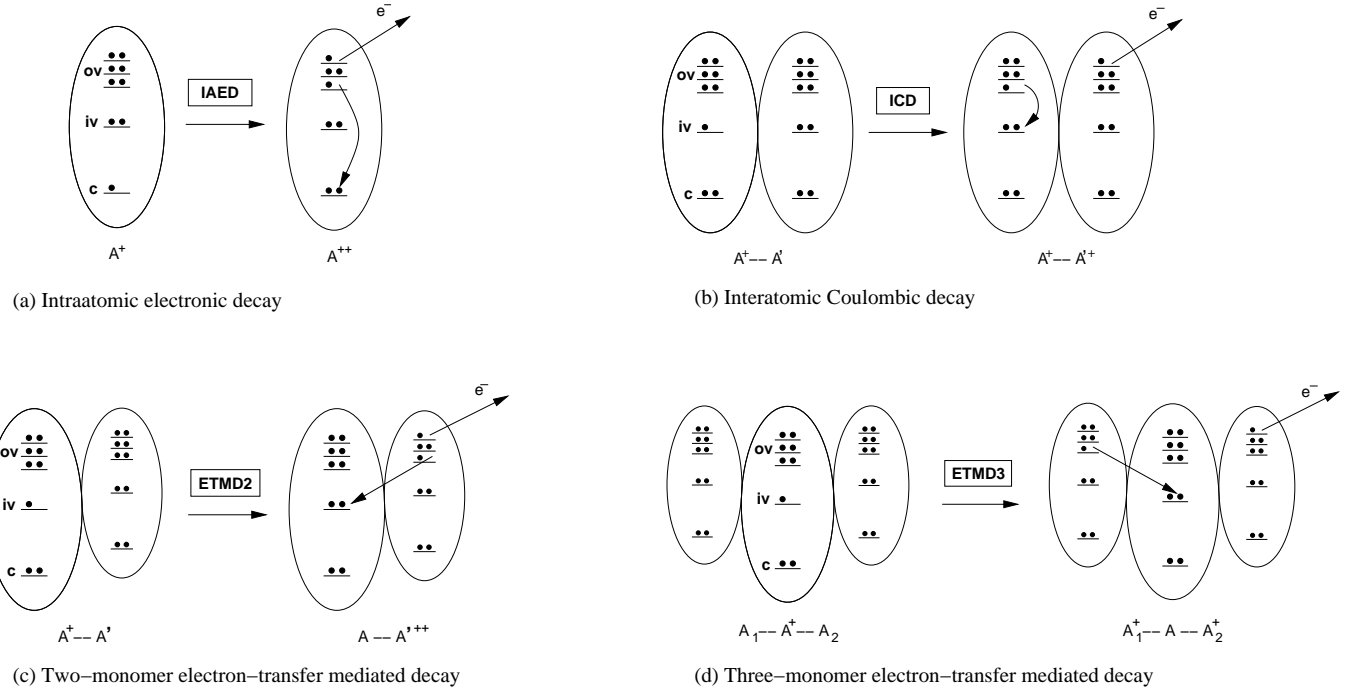


FIG. 2: Principles of electronic decay processes in weakly bound systems: (a) intra-atomic electronic decay (IAED), (b) interatomic Coulombic decay (ICD), (c) two-monomer electron-transfer mediated decay (ETMD2), (d) three-monomer electron-transfer mediated decay (ETMD3). Common to all electronic decay processes is that the initial vacancy is filled by a valence electron from the same or a neighboring atom. The excess energy is transferred to a second valence electron of the same or a neighboring atom. Emission of this electron results in distinct dicationic charge distributions that allow one to characterize the underlying decay process.

gested to occur for an initial $\text{Ne}2s$ vacancy in NeAr_2 .²⁶ A schematic representation of this (proposed) process is given in Fig. 2(d). A valence electron of one of the two argon atoms is transferred into the initial $\text{Ne}2s$ hole. Energy is released, and a valence electron is ejected from the second argon atom, leaving the trimer in a $\text{NeAr}^{-1}\text{Ar}^{-1}$ state.

We would like to study a new example for the surprising impact of the ideas presented so far. To this end, we examine the decay of $\text{Xe}4d$ vacancies in XeF_n and demonstrate how interatomic processes lead to an increase in Auger width. In order to pursue this issue, we need to introduce a few computational techniques and useful relations in the ensuing section.

III. COMPUTATIONAL METHODS AND BASIC RELATIONS

A. Algebraic Diagrammatic Construction and Two-Hole Population Analysis

Many-body Green's functions are ideal tools for investigating excitation spectra of molecular matter at various stages of ionization.^{41,42} The two-particle Green's function, specifically, provides direct access to double

ionization spectra and associated eigenstates. Algebraic diagrammatic construction (ADC) is an advanced perturbation-theoretical approximation scheme for evaluating many-body propagators.^{30,43,44,45} ADC(n) sums all Feynman diagrams up to n th order as well as certain classes of diagrams up to infinite order. There is no Dyson equation for the two-particle Green's function.^{46,47,48} The two-particle ADC evaluates the two-particle propagator directly in terms of a Hermitian eigenvalue problem.³⁰ The program⁴⁹ we use to calculate double ionization potentials implements the two-particle ADC(2) scheme.³⁰

The two-hole population analysis, utilized in combination with the ADC(2) program,⁴⁹ is a means to reveal the spatial localization of the two holes resulting from double ionization.^{14,31} The analysis is carried out in a Mulliken-type⁵⁰ fashion by determining the atomic two-hole ($2h$) contributions to the dicationic eigenstates. To this end, a dicationic eigenstate in the ADC(2) scheme is first expanded in terms of $2h$ configurations in molecular orbital basis,

$$|\Psi_n^{N-2}\rangle = \sum_{ij} (\vec{X}_n)_{ij} |ij\rangle + \dots, \quad (1)$$

where \vec{X}_n is the $2h$ part of the ADC eigenvector of the n th dicationic state $|\Psi_n^{N-2}\rangle$. The symbol $|ij\rangle$ denotes

a spin-adapted $2h$ configuration with holes in molecular (spin) orbitals i and j , both of which are occupied in the Hartree-Fock ground state of the N -electron system. Note that ij runs only over distinguishable $2h$ configurations. Each $2h$ configuration in molecular orbital basis, $|ij\rangle$, can now be expanded^{14,31} in terms of $2h$ configurations $|\mu\nu\rangle$ deriving from the atomic orbital basis

$$|ij\rangle = \sum_{\mu\nu} U_{\mu\nu,ij} |\mu\nu\rangle. \quad (2)$$

Using this transformation, the total $2h$ weight $\vec{X}_n^\dagger \vec{X}_n$ ($2h$ pole strength) of the n th dicationic eigenstate can be written as^{14,31}

$$\vec{X}_n^\dagger \vec{X}_n = \vec{Y}_n^\dagger \mathbf{O} \vec{Y}_n = \sum_{\mu\nu} \underbrace{\left[Y_{\mu\nu,n} \sum_{\rho\sigma} \mathbf{O}_{\mu\nu,\rho\sigma} Y_{\rho\sigma,n} \right]}_{Q_{\mu\nu,n}}, \quad (3)$$

with eigenvector expansion coefficients $\vec{Y}_n := \mathbf{U} \vec{X}_n$ in atomic orbital basis. \mathbf{O} represents the overlap matrix between atomic $2h$ configurations, which satisfies $\mathbf{U}^\dagger \mathbf{O} \mathbf{U} = \mathbb{1}$.

On choosing suitable sets of atomic basis functions A and B , one obtains population numbers^{14,31} $Q_{AB,n} = \sum_{\mu \in A, \nu \in B} Q_{\mu\nu,n}$. Frequently, as is done in this work, A and B represent the atomic basis functions associated with two not necessarily distinct atoms within a molecule. In this sense, A and B can be identified with individual atoms. This provides a clear picture of the localization properties of the two holes.

B. Relation between Two-Hole Population Numbers and Partial Decay Widths

A useful approximation to the decay width of a resonance is given within the framework of Wigner-Weisskopf theory,^{32,33} which is founded on time-dependent perturbation theory. Applications of Wigner-Weisskopf theory to the electronic decay of inner-valence-ionized clusters can be found in Refs. 28 and 26. There, single Hartree-Fock determinants were employed to describe both initial and final states. For more complicated systems like XeF_n and on the energy scale of core levels, however, the final states in particular require a more sophisticated treatment.

Let the initial state $|\Psi_1^{N-1}\rangle$ be a discrete, singly ionized state approximating the core-hole resonance and a final state be a doubly ionized state $|\Psi_n^{N-2}\rangle$ together with a decay electron of momentum \vec{k} . For simplicity we employ the sudden approximation (Ref. 51, and references therein) and express such a final state by the antisymmetrized product $\hat{c}_{\vec{k}}^\dagger |\Psi_n^{N-2}\rangle$, where $\hat{c}_{\vec{k}}^\dagger$ is a fermionic

creation operator.⁵² The decay width is then given by

$$\Gamma = 2\pi \sum_n \sum_{\vec{k}} |\langle \Psi_n^{N-2} | \hat{c}_{\vec{k}} \hat{H} | \Psi_1^{N-1} \rangle|^2 \delta(E_{n\vec{k}} - E_1). \quad (4)$$

This equation contains three types of matrix elements: transition matrix element $\langle \Psi_n^{N-2} | \hat{c}_{\vec{k}} \hat{H} | \Psi_1^{N-1} \rangle$; initial-state energy $E_1 := \langle \Psi_1 | \hat{H} | \Psi_1 \rangle$; and final-state energy $E_{n\vec{k}} := \langle \Psi_n^{N-2} | \hat{c}_{\vec{k}} \hat{H} \hat{c}_{\vec{k}}^\dagger | \Psi_n^{N-2} \rangle$. The operator \hat{H} is the Hamiltonian in fixed-nuclei approximation. The δ function in Eq. (4) ensures that the contribution to the total decay width of only those accessible final states is summed that conserve energy in the decay.

Using Eq. (1), we obtain

$$\langle \Psi_n^{N-2} | \hat{c}_{\vec{k}} \hat{H} | \Psi_1^{N-1} \rangle = \sum_{ij} (\vec{X}_n^\dagger)_{ij} \langle ij | \hat{c}_{\vec{k}} \hat{H} | \Psi_1^{N-1} \rangle + \dots \quad (5)$$

for the transition matrix elements in Eq. (4). Let us assume that the initial state can be approximated by a single determinant $|\Psi_1^{N-1}\rangle = \hat{c}_l |\Phi_0^N\rangle$, where l indicates a core orbital and $|\Phi_0^N\rangle$ the N -electron Hartree-Fock ground state. Let us further exploit the fact that excitations of core orbitals are, to a good approximation, negligible in all expansion terms of the dicationic final state $|\Psi_n^{N-2}\rangle$. The terms indicated in Eq. (5) with “ \dots ” then vanish exactly due to the Slater-Condon rules.⁵⁰

To proceed, we express the dicationic electronic configurations in terms of atomic $2h$ vectors $|\mu\nu\rangle$. The configurations $|ij\rangle$ appearing in Eq. (5) form an orthonormalized set of functions, and by using the relation

$$|ij\rangle = \sum_{\mu\nu, \rho\sigma} (\mathbf{O}^{\frac{1}{2}})_{\mu\nu, \rho\sigma} U_{\rho\sigma,ij} |\mu\nu\rangle, \quad (6)$$

we introduce an *orthonormalized* set of configurations $|\mu\nu\rangle$ referring to atomic orbitals. Notice that the atomic configurations in Eq. (2) are not orthonormalized. Inserting Eq. (6) into Eq. (5) leads to

$$\langle \Psi_n^{N-2} | \hat{c}_{\vec{k}} \hat{H} | \Psi_1^{N-1} \rangle = \sum_{\mu\nu} (\vec{Y}'_n)_{\mu\nu} \langle \mu\nu | \hat{c}_{\vec{k}} \hat{H} | \Psi_1^{N-1} \rangle, \quad (7)$$

where $\vec{Y}'_n := \mathbf{O}^{\frac{1}{2}} \mathbf{U} \vec{X}_n$. This equation relates the transition matrix element to a superposition of atomic-like quantities.

We now insert the transition matrix element (7) into the basic Eq. (4) for the decay width, integrate over the momentum \vec{k} of the emitted electron, and neglect interference terms (cross terms). The result reads

$$\begin{aligned} \Gamma &= \sum_n \Gamma_n, \\ \Gamma_n &= \sum_{\mu\nu} |T_{\mu\nu}|^2 |Y'_{\mu\nu,n}|^2. \end{aligned} \quad (8)$$

The partial width Γ_n associated with the final dicationic state $|\Psi_n^{N-2}\rangle$ is expressed as a sum over atomic $2h$ configurations. Each contributing term consists of a state-specific factor $|Y'_{\mu\nu,n}|^2$, which we have calculated earlier.

The other factor,

$$|T_{\mu\nu}|^2 = 2\pi \sum_{\vec{k}} |\langle \mu\nu | \hat{c}_{\vec{k}} \hat{H} | \Psi_{\text{I}}^{N-1} \rangle|^2 \delta(E_{n\vec{k}} - E_{\text{I}}), \quad (9)$$

depends on the dicationic state $|\Psi_n^{N-2}\rangle$ only via the δ function and is termed transition strength. Since we consider the decay of a core level, implying that the energy of the emitted electron is relatively high, this dependence on n is weak and can be neglected to a good approximation.

The state-specific quantities $|Y'_{\mu\nu,n}|^2$ are closely related to the occupation numbers discussed in Sec. III A. In principle, they could be used as an alternative definition of occupation numbers in the spirit of Löwdin's population analysis.⁵⁰ In particular, if the atomic basis functions are well localized, each on its atom, we may put $|Y'_{\mu\nu,n}|^2 = Q_{\mu\nu,n}$ and obtain

$$\Gamma_n = \sum_{\mu\nu} |T_{\mu\nu}|^2 Q_{\mu\nu,n}. \quad (10)$$

For a given molecule the quantities $|T_{\mu\nu}|^2$ are universal, and the only information that is state-specific is contained in the occupation numbers $Q_{\mu\nu,n}$. We are able to compute the occupation numbers of the molecules studied in this work, and hence Eq. (10) is already a useful tool of analysis.

We note, however, that many elements $|T_{\mu\nu}|^2$ can be of similar magnitude, e.g., if μ denotes a p -type atomic orbital on atom A and ν a p -type atomic orbital on atom B . We therefore group together in Eq. (10) the corresponding contributions: $\Gamma_n = |T_{AB}|^2 \sum_{\substack{\mu \in A \\ \nu \in B}} Q_{\mu\nu,n} + \dots$. Since

the $|T_{\mu\nu}|^2$ grouped together are not identical, the average quantity $|T_{AB}|^2$ will depend somewhat on the dicationic state index n . Computing $\Gamma = \sum_n \Gamma_n$ amounts to averaging over the slightly varying $|T_{AB}|^2$ and thus leads to a more stable result.

Highly localized dicationic final-state holes, for example those that result from ICD in weakly bound clusters, lead to similar contributions to the overall decay width of the initially ionized state. By classifying the atomic pairs $(\mu\nu)$ by their localization characteristics, we can form sets of atomic orbitals where $|T_{AB}|^2$ is only a slightly varying quantity. Let us denote with A the atom on which the initial core hole is localized. Then, if μ and ν denote atomic orbitals on A , $|T_{\mu\nu}|^2$ obviously corresponds to IAED (Sec. II). Analogously, if μ belongs to atom A and ν to atom B , we are dealing with ICD, and if neither μ nor ν belong to A , $|T_{\mu\nu}|^2$ describes either ETMD2 or ETMD3, depending on whether μ and ν belong to the same atom B or to two atoms B and C . Thus, the *minimal* dissection of Γ into its various contributions, in the spirit of the above discussion, reads

$$\Gamma = \Gamma_{\text{IAED}} + \Gamma_{\text{ICD}} + \Gamma_{\text{ETMD2}} + \Gamma_{\text{ETMD3}}, \quad (11)$$

where

$$\begin{aligned} \Gamma_{\text{IAED}} &= |T_{\text{IAED}}|^2 Q_{\text{IAED}}, \\ \Gamma_{\text{ICD}} &= |T_{\text{ICD}}|^2 Q_{\text{ICD}}, \\ \Gamma_{\text{ETMD2}} &= |T_{\text{ETMD2}}|^2 Q_{\text{ETMD2}}, \\ \Gamma_{\text{ETMD3}} &= |T_{\text{ETMD3}}|^2 Q_{\text{ETMD3}}, \end{aligned} \quad (12)$$

and

$$\begin{aligned} Q_{\text{IAED}} &= \sum_n \sum_{\mu, \nu \in A} Q_{\mu\nu,n}, \\ Q_{\text{ICD}} &= \sum_n \sum_{\substack{\mu \in A \\ \nu \in B}} Q_{\mu\nu,n}, \\ Q_{\text{ETMD2}} &= \sum_n \sum_{\substack{\mu, \nu \in B}} Q_{\mu\nu,n}, \\ Q_{\text{ETMD3}} &= \sum_n \sum_{\substack{\mu \in B \\ \nu \in C}} Q_{\mu\nu,n}. \end{aligned} \quad (13)$$

If necessary, further dissections of Γ into more detailed contributions are readily done. For instance, grouping together separately the contributions of μ and ν , both being atomic orbitals of s type, both of p type, or one of s and one of p type, etc. A distinction between the decay into singlet and triplet final dicationic states is also possible. Finally, we mention that the individual transition strengths, $|T_{\text{ICD}}|^2$, etc., may be similar in a series of related molecules.

IV. RESULTS AND DISCUSSION

A. Double Ionization Spectra

The computed double ionization spectra for the xenon atom, the fluorine molecule, and the series XeF_n , $n = 2, 4, 6$, are shown in Fig. 3. The molecular ground-state geometries used in the calculations are described in Refs. 21 and 22. It has to be stressed, however, that the double ionization spectrum of XeF_6 , unlike the single ionization spectrum in Refs. 21 and 22, has been calculated assuming a geometry of O_h symmetry, instead of C_{3v} symmetry, in order to make the calculation feasible with the available computer resources. We also refer the reader to Refs. 21 and 22 for details regarding the Gaussian basis sets employed.

The ADC 2h pole strength plotted in Fig. 3 characterizes how well the dicationic states are described by 2h configurations. The deviation of the 2h pole strength from unity yields the total contribution of three-hole-one-particle configurations to the state in question. Our focus in this work is on the energy regime below the $\text{Xe} 4d$ single ionization threshold, which ranges from almost 68 eV in atomic Xe to a little less than 76 eV in XeF_6 .^{19,21,22} The double ionization spectra below 80 eV in Fig. 3 comprise ionization out of the outer and inner valence of Xe, F_2 , and XeF_n . Since mean-field and correlation effects, as revealed by the ADC scheme, dominate

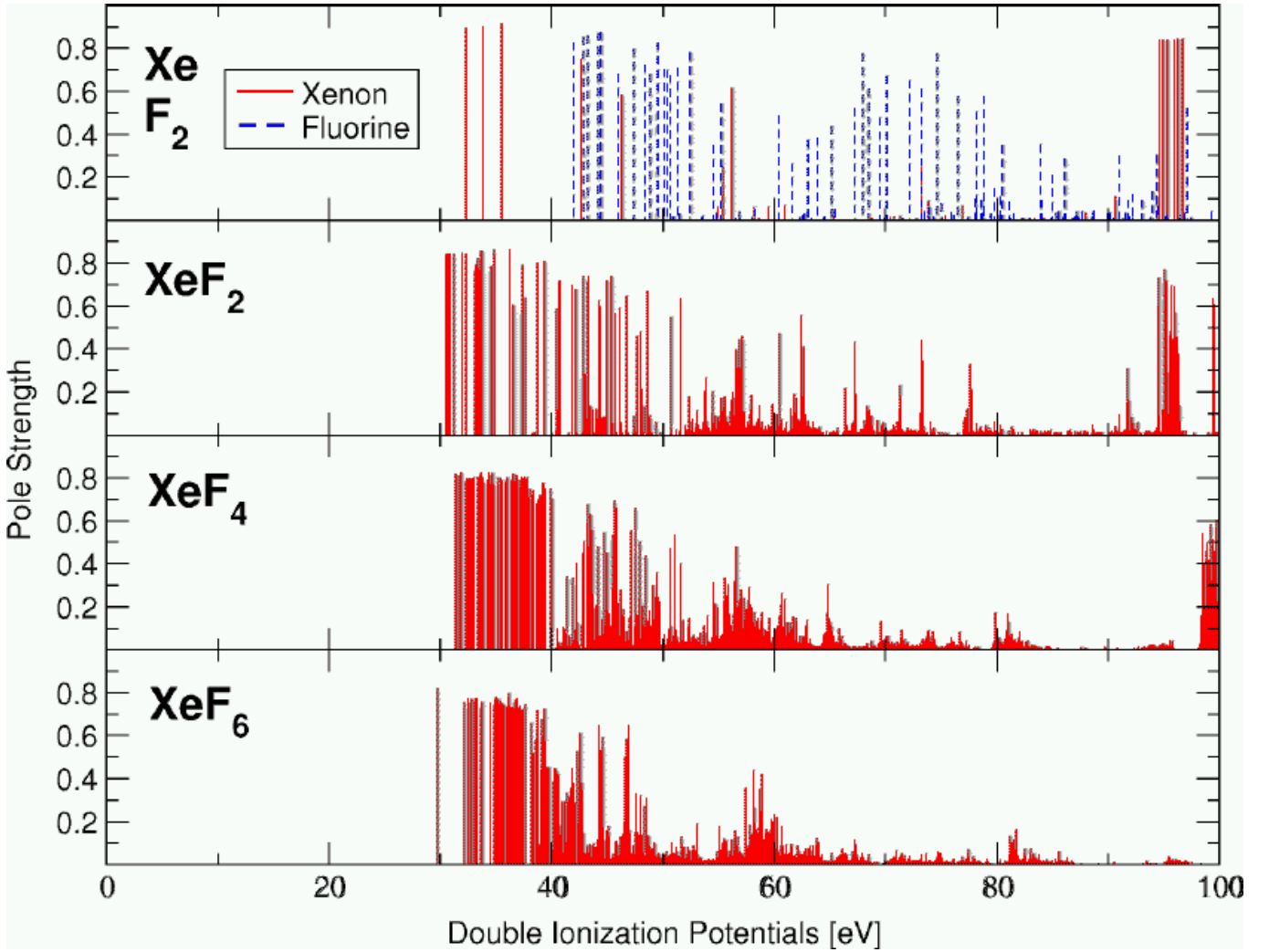


FIG. 3: (Color) Double ionization spectra of Xe, F_2 , XeF_2 , XeF_4 , and XeF_6 . The two-particle ADC(2) $2h$ pole strength is plotted on the ordinate to characterize how well the dicationic final states are described by $2h$ configurations.

in the valence region, the spectra have not been corrected for relativistic effects, which are expected to be negligible.

Double ionization from the outer valence of the xenon atom takes place between 30 and 40 eV, and three distinct DIPs are found in Fig. 3. The spectra of the series XeF_n , $n = 2, 4, 6$, display in this region increasingly dense lying DIPs, which is attributed to a growing number of outer-valence states due to a higher delocalization of the two final-state holes. The double ionization spectrum of F_2 in Fig. 3 shows outer-valence ionization of F_2 in the range between 40 and 55 eV. With an increasing number of fluorine ligands, the general trend in the spectra, especially at DIPs above 40 eV, is a decrease of the validity of the two-hole description of dicationic states of XeF_n . As all fluorine atoms in XeF_n are equivalent (the double ionization spectrum of XeF_6 is obtained in O_h symmetry), a dicationic state with a hole on xenon and a hole on a fluorine atom is in fact a linear combi-

nation of configurations involving a hole on xenon and a hole on one of the n fluorine atoms in XeF_n . The coefficients of the linear combinations are determined by the strength of the interaction among the fluorine ligands, being the weakest in XeF_2 .

The triple ionization threshold of the xenon atom⁵³ is 66.2 eV; for the xenon fluorides, the triple ionization threshold is at least that low. Therefore, many of the dicationic states we have calculated can decay to tricationic ones. Owing to the discrete basis set used, the appearance of a decaying state mimics a discretized Lorentzian curve.²⁵ As can be seen in Fig. 3, such curves may indeed be identified for XeF_n above 50 eV. Interestingly, the $Xe 4d$ lines in the single ionization spectra of xenon and its fluorides^{19,21,22} are thus above the triple ionization threshold. This indicates that there is some probability for the $Xe 4d$ holes to decay by emitting *two* electrons. According to a measurement by Kämmerling *et al.*,⁵⁴ this probability amounts to about 20 % in atomic xenon.

When analyzing the DIPs, one has to keep in mind that essentially there are four contributions to a dicationic state that determine its character. The two holes in the dicationic state can be localized on *one* atom, either Xe or F, or on *two* atoms, Xe and F or two different F atoms. The one-site states have a large dicationic population number on either xenon (Xe^{-2}) or a single fluorine (F^{-2}), and the two-site states are of either $\text{Xe}^{-1}\text{F}^{-1}$ or $\text{F}1^{-1}\text{F}2^{-1}$ character. For each dicationic state appearing in the spectra of the xenon fluorides, the data of the population analysis for equivalent fluorine atoms are summed up to yield the population numbers. In XeF_2 , for example, the $\text{Xe}^{-1}\text{F}1^{-1}$ and $\text{Xe}^{-1}\text{F}2^{-1}$ population numbers are added to give a single $\text{Xe}^{-1}\text{F}^{-1}$ contribution for each dicationic state in the spectrum of XeF_2 .

B. One-site Population Numbers

The one-site population numbers for the xenon fluorides are plotted in Fig. 4. For the graphical representation in Fig. 4 and in Fig. 5, the population numbers have been normalized, i.e., the sum of the contributions of Xe^{-2} , F^{-2} , $\text{Xe}^{-1}\text{F}^{-1}$, and $\text{F}1^{-1}\text{F}2^{-1}$ character equals unity for each dicationic eigenstate. The spectra are compared to study the effect of the increasing number of fluorine atoms. The first states in the double ionization spectra possess DIPs of ≈ 30 eV. The major contribution of the one-site population Xe^{-2} is at the lower energy part of the spectrum. Obviously, the density of states with a considerable F^{-2} population increases due to the increasing number of fluorine atoms. The overall distribution of these states does not change much in the different compounds. Certain regions are visible where the states have a high F^{-2} population. These regions shift slightly to higher DIPs due to the reduced excess charge that the individual fluorine atoms acquire from the central xenon atom in the molecular ground state.^{21,22}

Conversely, the importance of Xe^{-2} contributions to the dicationic states is extremely reduced due to the withdrawal of valence electron density on the xenon atom. In XeF_6 , the contributions of Xe^{-2} character have nearly vanished.

C. Two-site Population Numbers

The two-site population numbers for the xenon fluorides are plotted in Fig. 5. The impact of the increasing number of fluorine atoms is seen here as well. The states with a large $\text{F}1^{-1}\text{F}2^{-1}$ population in the spectrum of XeF_2 are clearly separated into distinct groups of lines originating from $\text{F}1\ 2p^{-1}\ \text{F}2\ 2p^{-1}$, $\text{F}1\ 2p^{-1}\ \text{F}2\ 2s^{-1}$, and $\text{F}1\ 2s^{-1}\ \text{F}2\ 2s^{-1}$ populations. This can be concluded from a simple energy consideration. The IPs for ionization from molecular orbitals with $\text{F}\ 2p$ character are located at ≈ 20 eV, those for ionization from molecular orbitals with $\text{F}\ 2s$ character are located at ≈ 40 eV.^{21,22}

In the spectrum of XeF_2 in Fig. 5, the groups are approximately at 40, 60, and 80 eV. XeF_2 is a linear molecule, the two fluorine atoms being separated by the central xenon atom. Such states with a large $\text{F}1^{-1}\text{F}2^{-1}$ population are termed *opposite* $\text{F}1^{-1}\text{F}2^{-1}$ states.

The situation changes in XeF_4 and XeF_6 . There are *adjacent* and opposite $\text{F}1^{-1}\text{F}2^{-1}$ states, and the clear separation between the groups seen in the spectrum of XeF_2 is lost. One reason for this effect is the interaction between adjacent fluorine atoms, which is stronger than the interaction between opposite ones. This leads to a splitting of the fluorine lines, which is also observed in the single ionization spectra.^{21,22}

The $\text{F}1\text{--F}2$ distance in adjacent $\text{F}1^{-1}\text{F}2^{-1}$ states is considerably reduced in comparison to the $\text{F}1\text{--F}2$ distance in opposite states, and the hole-hole repulsion energy varies accordingly. Of course, one has to compare states which have a large $\text{F}1^{-1}\text{F}2^{-1}$ population that arises from the same types of orbitals. Such $\text{F}1^{-1}\text{F}2^{-1}$ states are distributed over a small energy range in the double ionization spectrum. Corresponding lines in XeF_2 mark the lower ends of such DIP ranges, due to the maximum distance between the two vacancies. Coulomb repulsion between holes on adjacent fluorine ligands in XeF_4 and XeF_6 results in shifts toward higher DIPs.

States with a large $\text{Xe}^{-1}\text{F}^{-1}$ population do not group like those of $\text{F}1^{-1}\text{F}2^{-1}$ character. The density of these $\text{Xe}^{-1}\text{F}^{-1}$ states also increases with an increasing number of fluorine atoms, but they are distributed more uniformly over the whole spectral range. In XeF_2 and XeF_6 , these states are dominant with respect to population number, and in XeF_4 they are comparable to the $\text{F}1^{-1}\text{F}2^{-1}$ states. The DIPs of the $\text{Xe}^{-1}\text{F}^{-1}$ states are not subject to a change of the hole-hole repulsion energy (in contrast to those of the $\text{F}1^{-1}\text{F}2^{-1}$ states) because the $\text{Xe}\text{--F}$ distance is the same for all fluorine ligands within a molecule (remember that the double ionization spectrum of XeF_6 was calculated assuming octahedral symmetry).

D. $\text{Xe}\ 4d$ Linewidth

The electronic decay processes presented in Sec. II are characterized in Sec. III B according to their final-state population. Using Eqs. (11), (12), and (13), the analysis of the final-state population numbers allows one to determine the relative importance of IAED, ICD, ETMD2, and ETMD3 for the electronic decay of a $\text{Xe}\ 4d$ hole in XeF_n . The partial decay width associated with a given decay process can be viewed, according to Eq. (12), as a product of an averaged Coulomb matrix element and a two-hole population factor related to that process.

We calculated the population factors, as defined by Eq. (13), by summing population numbers up to the energy of the $\text{Xe}\ 4d$ lines obtained in Ref. 22. The results are collected in Table I. We see that Q_{IAED} is rather low in the xenon fluorides, especially when compared to the

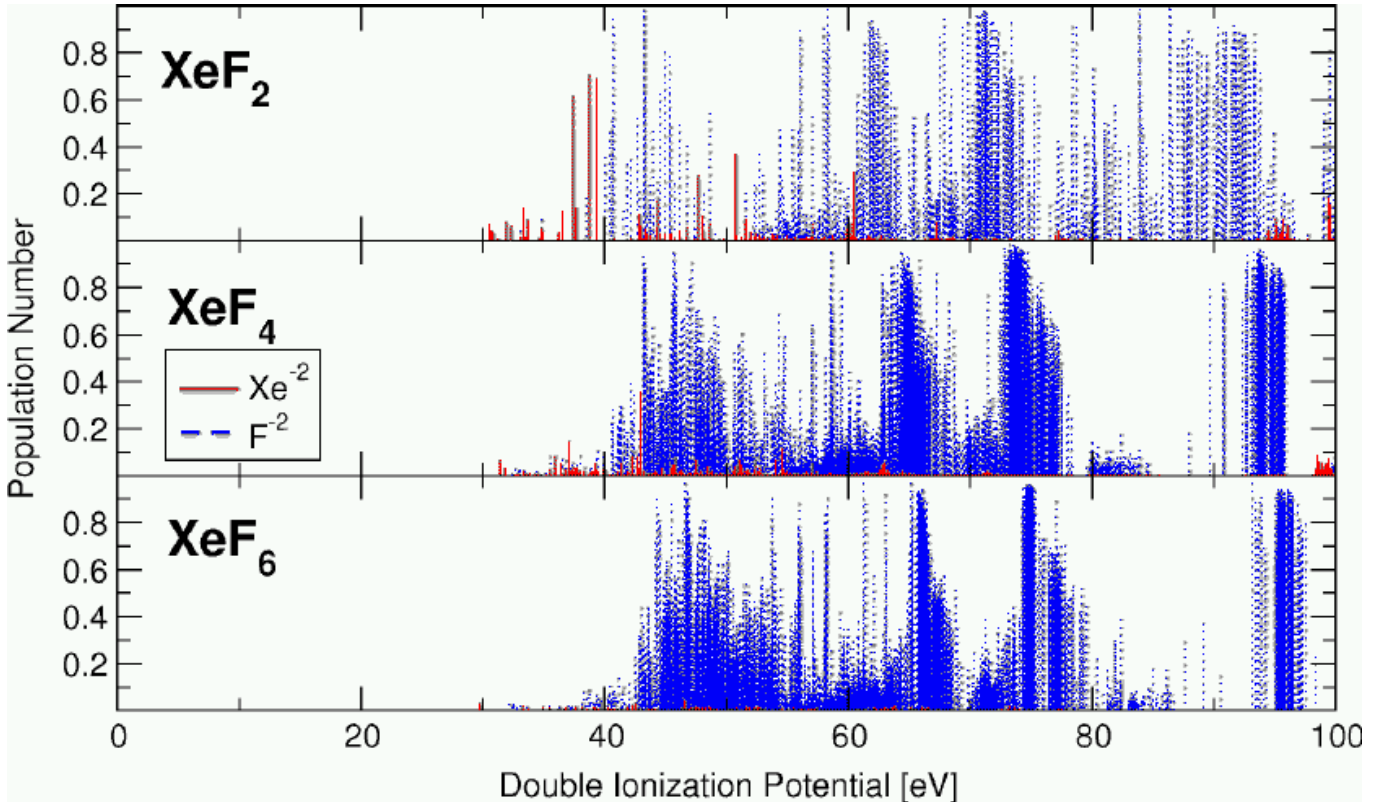


FIG. 4: (Color) One-site population numbers of the double ionization spectra of XeF_2 , XeF_4 , and XeF_6 . Each line shown is related to a dicationic state in the double ionization spectra in Fig. 3. The height of the line gives the one-site population number. Note that the contributions on xenon decrease drastically as the number of fluorine atoms increases.

Compound	Q_{IAED}	Q_{ICD}	Q_{ETMD2}	Q_{ETMD3}
Xe	14.6	0	0	0
XeF_2	10.4	43.8	19.4	22.7
XeF_4	7.1	68.1	34.3	124.1
XeF_6	4.8	80.2	45.5	288.6

TABLE I: Two-hole population factors for intra-atomic electronic decay (IAED) and for the interatomic decay processes ICD, ETMD2, and ETMD3 in xenon and its fluorides. The two-hole population factors are defined in Eq. (13).

population factors Q_{ICD} , Q_{ETMD2} , and Q_{ETMD3} . Hence, as far as population numbers are concerned, IAED is suppressed, and interatomic decay processes dominate the electronic decay of a $\text{Xe} 4d$ hole. Also note the sensitive dependence of all population factors on the number of fluorine ligands.

In order to arrive at a complete picture, the transition strengths in Eq. (12) have to be determined. For this purpose, we make a reasonable assumption: The transition strengths $|T_{\text{IAED}}|^2$, $|T_{\text{ICD}}|^2$, $|T_{\text{ETMD2}}|^2$, and $|T_{\text{ETMD3}}|^2$ are universal for xenon and its fluorides. This allows us—utilizing Eqs. (11) and (12)—to take the averaged experimental $\text{Xe} 4d$ linewidths, displayed in Fig. 1 and

reproduced in Table III, and the population factors in Table I to set up a linear system of four equations for the four unknown transition strengths. The matrix of population factors, however, is extremely ill-conditioned, as its \mathbb{L}^2 condition number,⁵⁵ for instance, is 945, which is much larger than unity. This means that the solution of the linear system depends strongly on the accuracy of the population factors.

Therefore, we first determine $|T_{\text{IAED}}|^2$ by solving Eqs. (11) and (12) for the xenon atom. We then exploit that both $|T_{\text{ETMD2}}|^2$ and $|T_{\text{ETMD3}}|^2$ are based on electron transfer between Xe and a fluorine ligand. They are thus expected to be of similar magnitude, so we set $|T_{\text{ETMD2}}|^2 = |T_{\text{ETMD3}}|^2$. The remaining linear system of three equations and two unknowns can be solved in a stable fashion by a least-squares procedure.⁵⁵ The calculated transition strengths for Xe and XeF_n are displayed in Table II. The results are in line with expectations: The transition strength associated with intra-atomic decay is greater by an order of magnitude than the interatomic energy-transfer strength of ICD. $|T_{\text{ETMD2}}|^2$ and $|T_{\text{ETMD3}}|^2$, which require interatomic orbital overlap for electron transfer, are even smaller.

Finally, by combining the population factors from Table I and the transition strengths from Table II, the par-

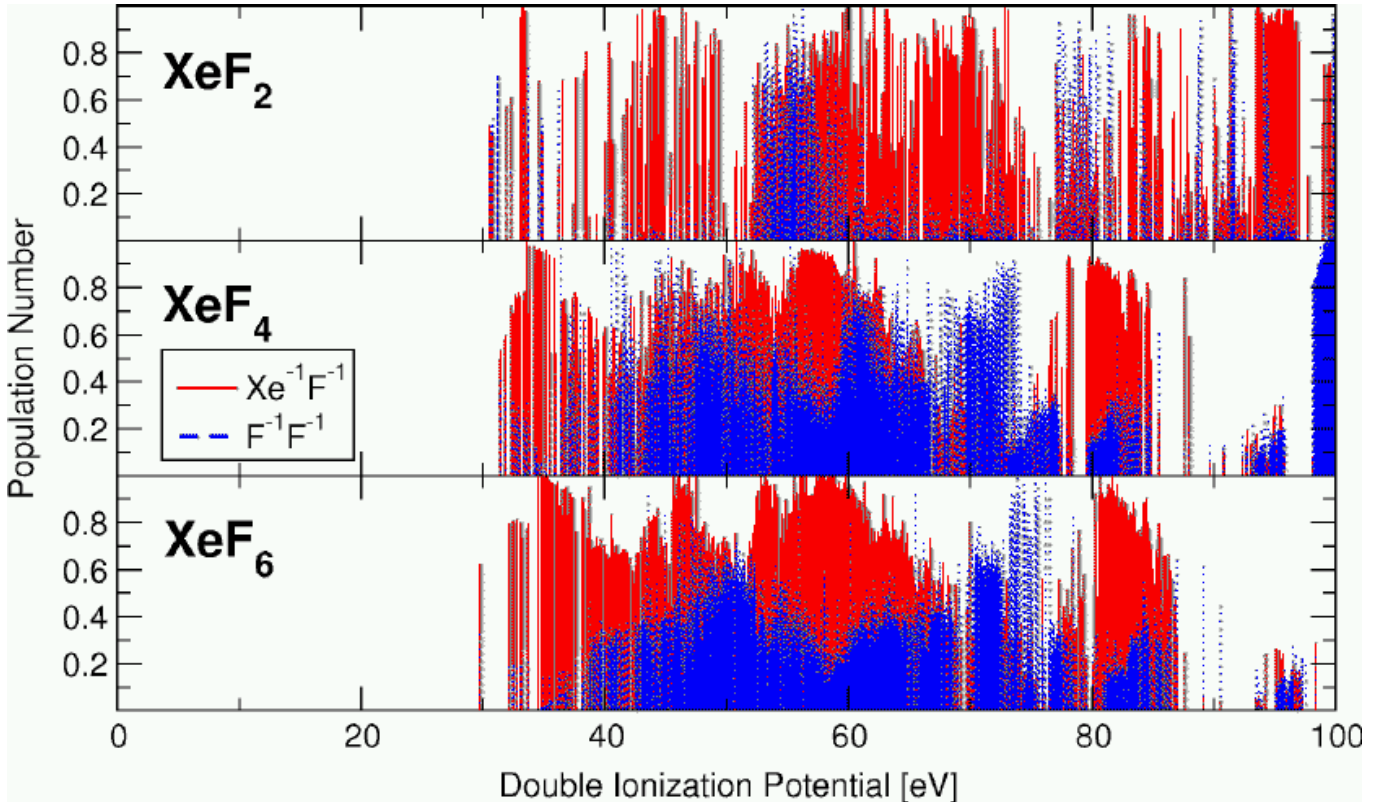


FIG. 5: (Color) Two-site population of the double ionization spectra of XeF_2 , XeF_4 , and XeF_6 .

Decay Process	$ T ^2$ [eV]
IAED	1.4×10^{-2}
ICD	1.9×10^{-3}
ETMD2/ETMD3	2.1×10^{-4}

TABLE II: Transition strengths for electronic decay of a $\text{Xe}4d$ hole in XeF_n .

tial widths Γ_{IAED} , Γ_{ICD} , Γ_{ETMD2} , and Γ_{ETMD3} in XeF_n can be computed [Eq. (12)]. They are presented in Table III. The conclusions that can be drawn from this table are truly remarkable. From Xe to XeF_6 , the contribution from IAED to the total $\text{Xe}4d$ decay width drops monotonically, consistent with the one-center picture mentioned in Sec. I. However, that decrease is more than compensated for by interatomic decay, which is the reason why an overall increase in $\text{Xe}4d$ width is observed in experiment. ICD is the most important interatomic decay mechanism. In XeF_4 , Γ_{ICD} is already greater than Γ_{IAED} , and in XeF_6 , more than 50 % of the total $\text{Xe}4d$ width are caused by ICD. Decay via electron transfer is less significant. Nevertheless, while ETMD2 is practically negligible throughout, Γ_{ETMD3} and Γ_{IAED} in XeF_6 are in fact comparable, due to the steep rise of the population factor Q_{ETMD3} between XeF_2 and XeF_6 (Table I).

V. CONCLUSION

We have shown that interatomic electronic decay processes are of prime importance for understanding relaxation of a $\text{Xe}4d$ vacancy in the xenon fluorides. The experimentally observed trend of increasing Auger width in the series XeF_n , $n = 0, 2, 4, 6$, is an impressive consequence of the fact that interatomic Coulombic decay and electron-transfer mediated decay not only cancel out the drop in intra-atomic Auger rate: Interatomic decay dominates by far in the larger xenon fluorides. In XeF_6 , for example, 76 % of the total $\text{Xe}4d$ linewidth is due to the combined effect of ICD, ETMD2, and ETMD3.

ICD in XeF_n takes place on an ultrashort time scale of less than 10 fs. This is of the same order of magnitude as the ICD lifetimes calculated for a $2s$ hole in a Ne atom surrounded by at least six neon monomers.²⁸ Our finding that, in XeF_6 , Γ_{ICD} is only a little more than two times greater than Γ_{ETMD3} , affords a new impulse for cluster and condensed-matter research. We anticipate ETMD3 to be a major decay mechanism for an inner-valence hole, for instance, in a neon atom embedded in an argon matrix.

There are obvious consequences of our investigation for molecules bearing a similarity to XeF_n . An interesting example is Auger decay of a $\text{Si}2p$ hole in SiF_4 . It was shown in Refs. 15 and 16 that virtually not a single di-

Compound	Γ_{IAED} [eV]	Γ_{ICD} [eV]	Γ_{ETMD2} [eV]	Γ_{ETMD3} [eV]	Γ_{expt} [eV]
Xe	0.20	0	0	0	0.20
XeF ₂	0.15	0.08	0.00	0.00	0.24
XeF ₄	0.10	0.13	0.01	0.03	0.26
XeF ₆	0.07	0.15	0.01	0.06	0.29

TABLE III: Decomposition of the mean experimental electronic decay width, Γ_{expt} , of the Xe 4d-lines in Xe and XeF_n into contributions from intra-atomic and interatomic decay processes. Γ_{expt} is taken from Fig. 1.

cationic (valence) eigenstate in SiF₄ is, at a significant level, of Si⁻² character. The occurrence of primarily multi-center decay channels is termed *foreign imaging*. It is these channels to which ICD, ETMD2, and ETMD3 provide access. In light of the present study, we may conclude that the calculation by Larkins,⁵⁶ based on the one-center model, must be expected to appreciably underestimate the Si 2p Auger width in SiF₄. A recent measurement by Thomas *et al.*¹⁸ proves this expectation to be justified: The experimental Si 2p Auger width is more than five times greater than the prediction of the one-center model. The authors of Ref. 18 also interpret this discrepancy in terms of interatomic electronic processes.

Our approach to molecular Auger decay, as presented in this paper, lays its emphasis on the decay channels. Though not impossible, an actual computation of Auger widths in such complicated many-electron systems as the xenon fluorides still cannot be carried out in a very reliable and accurate manner. We therefore put to use two highly powerful theoretical tools: the ADC scheme for the two-particle propagator and the two-hole population analysis of dicationic eigenstates. These two methods allow us to concentrate on the mechanisms underlying Auger decay by yielding detailed information about the nature of the available decay channels.

The key relations (11), (12), and (13) between two-

hole population numbers and partial Auger widths are, strictly speaking, only valid for molecules with pronounced charge localization characteristics. The xenon fluorides satisfy this criterion well. We are convinced, however, that the basic picture is much more general. In order to understand Auger decay in arbitrary molecules, it is usually insufficient to restrict the analysis to local valence electron densities. The physics may be even more complicated, but a qualitative decomposition into interatomic processes ICD, ETMD2, and ETMD3 is most likely still possible.

Acknowledgments

The authors are highly indebted to T. Darrah Thomas for pointing out Ref. 19 and supporting it further with valuable private communications (Fig. 1). This work would not have been possible without the ADC programs and support by Francesco Tarantelli. Imke B. Müller, Sven Feuerbacher, Jörg Breidbach, and Thomas Sommerfeld accompanied our work with helpful comments and fruitful discussions. R.S. and L.S.C. gratefully acknowledge financial support by the Deutsche Forschungsgemeinschaft (DFG).

* Author to whom all correspondence should be addressed; electronic mail: Christian.Buth@web.de; Present address: Max-Planck-Institut für Physik komplexer Systeme, Nöthnitzer Straße 38, 01187 Dresden, Germany

† Present address: JILA, University of Colorado, Boulder, CO 80309-0440

¹ P. Auger, Compt. Rend. (Paris) **177**, 169 (1923).

² E. H. Burhop, ed., *The Auger Effect and Other Radiationless Transition*, Cambridge Monographs on Physics (Krieger Publishing Company, Melbourne, 1980), ISBN 0-88275-966-3, reprint.

³ M. Thompson, M. D. Baker, J. F. Tyson, and A. Christie, *Auger Electron Spectroscopy*, Chemical Analysis Monographs (John Wiley & Sons, New York, 1985), ISBN 0-471-04377-X.

⁴ W. Bambynek, B. Crasemann, R. W. Fink, H. U. Freund, H. Mark, C. D. Swift, R. E. Price, and P. V. Rao, Rev. Mod. Phys. **44**, 716 (1972).

⁵ W. Bambynek, B. Crasemann, R. W. Fink, H. U. Freund, H. Mark, C. D. Swift, R. E. Price, and P. V. Rao, Rev.

Mod. Phys. **46**, 853 (1974).

⁶ H. Wormeester, H. J. Borg, and A. v. Silfhout, Surf. Sci. **258**, 197 (1991).

⁷ R. W. Shaw, Jr. and T. D. Thomas, Phys. Rev. Lett. **29**, 689 (1972).

⁸ R. M. Friedman, J. Hudis, and M. L. Perlman, Phys. Rev. Lett. **29**, 692 (1972).

⁹ M. Coville and T. D. Thomas, Phys. Rev. A **43**, 6053 (1991).

¹⁰ P. H. Citrin, Phys. Rev. Lett. **31**, 1164 (1973).

¹¹ Y. Yafet and R. E. Watson, Phys. Rev. B **16**, 895 (1977).

¹² T. A. Green and D. R. Jennison, Phys. Rev. B **36**, 6112 (1987).

¹³ J. A. D. Matthew and Y. Komminos, Surf. Sci. **53**, 716 (1975).

¹⁴ F. Tarantelli, A. Sgamellotti, and L. S. Cederbaum, J. Chem. Phys. **94**, 523 (1991).

¹⁵ F. Tarantelli and L. S. Cederbaum, Phys. Rev. Lett. **71**, 649 (1993).

¹⁶ F. O. Gottfried, L. S. Cederbaum, and F. Tarantelli, Phys.

Rev. A **53**, 2118 (1996).

¹⁷ T. X. Carroll, K. J. Børve, L. J. Sæthre, J. D. Bozek, E. Kukk, J. A. Hahne, and T. D. Thomas, J. Chem. Phys. **116**, 10221 (2002).

¹⁸ T. D. Thomas, C. Miron, K. Wiesner, P. Morin, T. X. Carroll, and L. J. Sæthre, Phys. Rev. Lett. **89**, 223001 (2002).

¹⁹ J. N. Cutler, G. M. Bancroft, J. D. Bozek, K. H. Tan, and G. J. Schrobilgen, J. Am. Chem. Soc. **113**, 9125 (1991).

²⁰ T. D. Thomas (private communication), based on data taken from Ref. 19.

²¹ C. Buth, Diplomarbeit, Ruprecht-Karls-Universität Heidelberg, Theoretische Chemie, Physikalisch-Chemisches Institut, Im Neuenheimer Feld 229, 69120 Heidelberg, Germany, 2002, www.ub.uni-heidelberg.de/archiv/3004.

²² C. Buth, R. Santra, and L. S. Cederbaum, J. Chem. Phys. **119**, 7763 (2003), arXiv: physics/0306123.

²³ L. S. Cederbaum, J. Zobeley, and F. Tarantelli, Phys. Rev. Lett. **79**, 4778 (1997).

²⁴ R. Santra, J. Zobeley, L. S. Cederbaum, and N. Moiseyev, Phys. Rev. Lett. **85**, 4490 (2000).

²⁵ J. Zobeley, L. S. Cederbaum, and F. Tarantelli, J. Chem. Phys. **108**, 9737 (1998).

²⁶ J. Zobeley, R. Santra, and L. S. Cederbaum, J. Chem. Phys. **115**, 5076 (2001).

²⁷ R. Santra, J. Zobeley, L. S. Cederbaum, and F. Tarantelli, J. Electron Spectrosc. Relat. Phenom. **114–116**, 41 (2001).

²⁸ R. Santra, J. Zobeley, and L. S. Cederbaum, Phys. Rev. B **64**, 245104 (2001).

²⁹ S. Marburger, O. Kugeler, U. Hergenhahn, and T. Möller, Phys. Rev. Lett. **90**, 203401 (2003).

³⁰ J. Schirmer and A. Barth, Z. Phys. A **317**, 267 (1984).

³¹ F. Tarantelli, A. Sgamellotti, and L. S. Cederbaum, in *Applied Many-Body Methods in Spectroscopy and Electronic Structure*, edited by D. Mukherjee (Plenum Press, New York, 1992), pp. 57–104, ISBN 0-306-44193-4.

³² J. J. Sakurai, *Modern Quantum Mechanics* (Addison-Wesley, Reading (Massachusetts), 1994), 2nd ed., ISBN 0-201-53929-2.

³³ V. F. Weisskopf and E. P. Wigner, Z. Phys. **63**, 54 (1930).

³⁴ R. Santra and L. S. Cederbaum, Phys. Rev. Lett. **90**, 153401 (2003).

³⁵ R. Santra, L. S. Cederbaum, and H.-D. Meyer, Chem. Phys. Lett. **303**, 413 (1999).

³⁶ J. Zobeley, L. S. Cederbaum, and F. Tarantelli, J. Phys. Chem. A **103**, 11145 (1999).

³⁷ S. Scheit, L. S. Cederbaum, and H.-D. Meyer, J. Chem. Phys. **118**, 2092 (2003).

³⁸ R. Santra, J. Zobeley, and L. S. Cederbaum, Chem. Phys. Lett. **324**, 416 (2000).

³⁹ I. B. Müller, J. Zobeley, and L. S. Cederbaum, J. Chem. Phys. **117**, 1085 (2002).

⁴⁰ R. Santra and L. S. Cederbaum, Phys. Rep. **368**, 1 (2002).

⁴¹ L. S. Cederbaum and W. Domcke, in *Adv. Chem. Phys.*, edited by I. Prigogine and S. A. Rice (John Wiley & Sons, New York, 1977), vol. 36, pp. 205–344.

⁴² L. S. Cederbaum, in *Encyclopedia of Computational Chemistry*, edited by P. v. R. Schleyer (John Wiley & Sons, Chichester, New York, 1998), vol. 2, pp. 1202–1211, ISBN 0-471-96588-X.

⁴³ J. Schirmer, Phys. Rev. A **26**, 2395 (1982).

⁴⁴ J. Schirmer, L. S. Cederbaum, and O. Walter, Phys. Rev. A **28**, 1237 (1983).

⁴⁵ J. Schirmer and G. Angonoa, J. Chem. Phys. **91**, 1754 (1989).

⁴⁶ J. Brand and L. S. Cederbaum, Ann. Phys. (New York) **252**, 276 (1996).

⁴⁷ J. Brand and L. S. Cederbaum, Phys. Rev. A **57**, 4311 (1998).

⁴⁸ J. Brand and L. S. Cederbaum, Adv. Quantum Chem. **38**, 65 (2001).

⁴⁹ F. Tarantelli (private communication).

⁵⁰ A. Szabo and N. S. Ostlund, *Modern Quantum Chemistry: Introduction to Advanced Electronic Structure Theory* (Macmillan, New York, 1982), ISBN 0-02-949710-8.

⁵¹ L. Hedin and J. D. Lee, J. Electron Spectrosc. Relat. Phenom. **124**, 289 (2002).

⁵² A. L. Fetter and J. D. Walecka, *Quantum Theory of Many-Particle Systems*, International Series in Pure and Applied Physics, edited by Leonard I. Schiff (McGraw-Hill, New York, 1971).

⁵³ D. Mathur and C. Badrinathan, Phys. Rev. A **35**, 1033 (1987).

⁵⁴ B. Kämmerling, B. Krässig, and V. Schmidt, J. Phys. B **25**, 3621 (1992).

⁵⁵ G. H. Golub and C. F. van Loan, *Matrix Computations* (John Hopkins University Press, Baltimore, 1989), 2nd ed., ISBN 0-8018-3772-3.

⁵⁶ F. P. Larkins, J. Electron Spectrosc. Relat. Phenom. **67**, 159 (1994).